Experimental Thermal and Fluid Science 150 (2024) 111052

Contents lists available at ScienceDirect

Experimental Thermal and Fluid Science

journal homepage: www.elsevier.com/locate/etfs

Enhancement of microchannel heat sink heat transfer: Comparison between different heat transfer enhancement strategies

G. Marseglia [a], M.G. De Giorgi [a], P. Pontes [b], R. Solipa [b], R.R. Souza [b,c], A.L.N. Moreira [b], A.S. Moita [b,d,*]

[a] University of Salento, Department of Engineering for Innovation, Via Per Monteroni, Lecce 73100, Italy
[b] IN+ Center for Innovation, Technology and Policy Research, Instituto Superior Técnico, Universidade de Lisboa, Portugal
[c] Metrics, Mechanical Engineering Department, University of Minho, Campus de Azurém, 4800-058 Guimarães, Portugal
[d] CINAMIL – Military Academy Research Center, Portuguese Military Academy, Amadora, Portugal

ARTICLE INFO

Keywords:
Cooling
Heat sink
Heat transfer
Microchannel
Nanofluid

ABSTRACT

This paper investigates the advantages and challenges associated with two-phase flows, specifically flow boiling of pure liquids and nanofluids, for cooling applications in microchannel heat sinks. The study explores various two-phase flow patterns, their related issues, and examines the potential of nanoparticles to enhance heat transfer. Alumina (Al_2O_3), gold (Au), and silver (Ag) nanoparticles at different concentrations were tested. Experimental tests were conducted under different working conditions using various working fluids, including water, Al_2O_3 1 wt%, Ag 1 wt%, Au 1 wt%, Au 0.75 wt%, Au 0.5 wt%. The heat fluxes used were 1.026 kW/m^2, 1.696 W/m^2 and 2.403 kW/m^2, while the volumetric flows ranged between 0.5 mL/min and 1.5 mL/min. The observed results indicate that even for the lowest particle concentration tested, the water-Au nanofluid exhibits superior cooling performance compared to the other examined fluids. The findings suggest that although two-phase flow conditions may not yield significant benefits, even small concentrations of nanoparticles ($\phi \ll 1\%$) can significantly impact heat transfer mechanisms. This approach provides a cost-effective and efficient alternative for cooling microchannel heat sinks without necessitating the use of two-phase flow conditions.

1. Introduction

Over the past few years, aerospace, aviation, defense, and military sectors have been among the most demanding, seeking solutions that are both lightweight and efficient while withstanding harsh environmental conditions and requiring minimal maintenance and cost.

However, the pressing challenge facing these industries today is to develop aviation defense devices that are more sustainable and have minimal environmental impact. Unmanned Aerial Vehicles (UAVs) – have become increasingly important in aerospace and defense aviation applications. UAVs are being used for a large range of applications, being used for intelligence, surveillance and reconnaissance military operations, network nodes, communication relays. In fact, in UAVs were the main drivers of drones' applications in the US [1–2]. As these systems become smaller and more complex, challenges arise in terms of heat dissipation.

As a result, the development of micro-electromechanical systems (MEMS) has garnered increased attention focusing on the coupling process of solid heat conduction and fluid convection or boiling heat transfer for improving temperature uniformity and minimizing the heat accumulation in the microsystems [3–6].

Microchannel Heat Sinks (MCHSs) are innovative micro-systems that have the ability to efficiently dissipate large amounts of heat within a small volume. This is achieved through a large surface area exposed to the convective and/or nucleate heat transmission processes. MCHS are particularly useful for high-integrated level and power applications [3,7–12], where enhanced heat transfer performance can lead to weight minimization. Due to these promising advantages, MCHSs are becoming increasingly popular in aircraft and aerospace cooling systems [13].

The dissipation of large amounts of heat continues to be a critical area of research, driving researchers to explore different cooling methodologies. [14–15].

Recent studies have concentrated on optimizing the geometric features of the microchannel structures [16]. For instance, Tuckerman and Pease [17] performed an optimization study on a rectangular shaped MCHS and demonstrated a reduction in thermal resistance during heat transfer. Additionally, other researchers have examined the potential to

* Corresponding author at: IN+ Center for Innovation, Technology and Policy Research, Instituto Superior Técnico, Universidade de Lisboa, Portugal.
E-mail address: anamoita@tecnico.ulisboa.pt (A.S. Moita).

https://doi.org/10.1016/j.expthermflusci.2023.111052
Received 14 March 2023; Received in revised form 27 July 2023; Accepted 3 September 2023
Available online 4 September 2023

Nomenclature

Greek symbols

β_{eff}	Thermal expansion
k	Thermal conductivity coefficient
Δp	pressure losses
μ	Molecular viscosity coefficient
ρ	Density
σ	Surface tension
τ	shear stress on the tube walls

Roman symbols

Ag	silver
Al	Alumina
AR	aspect ratio
Au	gold
C_p	Specific heat
D_h	hydraulic diameter
h_{fg}	Latent heat
H	height of the microchannel heat sink
H_c	height of the channel
L	length of the microchannel heat sink
p	Pressure.
P_p	pumping power
$\dot{Q}_i$	volumetric flow rate
q"	surface heat flux
Nu	Nusselt number
Pr	Pradtl number
Pe	Peclet number
Re	Reynolds number
SD	standard deviation
t	substrate thickness of the microchannel heat sink
T_{in}	liquid temperature at the entrance
T_{out}	liquid temperature at the exit
u	Velocity vector.
u_m	mean flow velocity
u,v,w	Velocity Cartesian components
W	width of the microchannel heat sink
w_c	channel width
w_w	wall width

Subscripts

amb	ambient condition.
i,j,k	Computational indexes.
n	Normal component.
n_f	stands for nanofluid
$n_{p.}$	stands for nanoparticle
x,y,z	Cartesian components.

Acronyms

HFE	hydrofluoroether
MCHs	Microchannel Heat sinks
MEMS	micro-electromechanical systems
PLA	polylactic acid
UAVs	Unmanned Aerial Vehicles

enhance thermo-hydraulic efficiency by considering the interlaced structure and the geometric characteristics of MCHs [18].

Introducing two-phase flow is another popular strategy. To enhance the performance of microchannel heat sinks. Wambsganss *et al.* [19] were among the first to apply two-phase flow to the microchannel heat sinks, which has since been a popular research area for optimizing their efficiency. However, this method has its downsides, as it consumes energy and is prone to instabilities caused by bubbles making it difficult to control and understand. To improve the efficiency of microchannel heat sinks, various authors have explored different geometries, surfaces, and working fluids, including Lee and Mudawar [20], Li *et al.* [21] and Ma *et al.* [22]. Some authors, like [19], Harirchian and Garimella [23] and Kandlikar [24,25] studied the patterns of flow boiling found in their experiments, which was used as reference for the findings of the present work.

The need to understand the dynamics of the bubbles through a more systematic experimental approach has arisen in order to customize the design of heat sinks using flow boiling in microchannels.

Alternatively, nanofluids have been labelled as an excellent alternative to conventional heat transfer fluids for conserving energy in several applications, such as in aerospace sector [26–27] or renewable energies in solar aircraft [28]. Nanofluids, which are specially designed to transfer heat energy, consist of nanomaterials that are uniformly distributed in the medium, with sizes ranging from 1 to 100 nm, and a base fluid, forming nanoscale colloidal suspensions containing condensed nanomaterials. These fluids possess the unique ability to enhance thermophysical properties such as thermal conductivity, thermal diffusivity, viscosity, and convective heat transfer coefficients when compared to their base fluids, such as oil or water [29–32].

As a result of this breakthrough, nanotechnology has taken over a major portion of convective heat transfer engineering and is being used in the study of thermal transport along a nanoscale flow of matter [33–42]. Some properties of nanofluids are dependent on their preparation method and stability. Achieving the desired stability remains a significant challenge in nanofluid technology.

The capability to enhance heat flux exchange using nanofluids was first considered by Choi and Eastman [43] in 1995, analyzing the behavior of metallic nanometer particles in water. They studied the thermal conductivity behavior based on the Hamilton and Crosser model [44] and on some experimental tests developed by Masuda et al. [45] considering nanoparticles of γ-Al_2O_3 and water. Subsequent studies have further demonstrated the potential of nanofluids to enhance heat transfer. For example, a numerical study on nanofluid thermal performance developed by [46] considering different types of nanoparticles (CuO, Al_2O_3, Ag, Cu, TiO_2) highlighted that a higher percentage of nanoparticles in base fluid can enhance the Nusselt number. Esmaeili et al. [47] demonstrated improved heat transfer rates in sinusoidal wave shaped channels with the addition of alumina (Al_2O_3) nanoparticles to water. Yang et al. [48] investigated the convective resistance of the nanofluid in the recirculation zone of backward-facing step microchannels. In their work they considered nanoparticles of TiO_2, SiO_2 and Al_2O_3 used in volume concentrations ranging from 0.1% to 0.3% and analyzed the heat flux exchange and the flow resistance features of the considered nanofluids. Kherbeet et al. [49] examined SiO_2 nanofluids with volume fractions of 0.5% and 1% (diameter of 30 nm), obtaining a high value of the heat transfer coefficients in the case of the nanofluids with higher nanoparticle concentration. Ozbolat et al. [50] investigated the effects of various geometry features on the improvement of the heat transfer coefficient using Al_2O_3 nanofluids.

Recently more researchers are focusing the attention on a new generation of nanofluids, the so-called "hybrid nanofluids" that allow to enhance the thermal properties of the fluid thanks to their possible synergistic effects between nanoparticles [51–56].

Obviously, further investigations that compare convection mechanisms within hybrid nanofluids and equivalent mono nanofluids are required, to deepen the knowledge of these phenomena, especially under turbulent flow conditions.

Vallejo et al. [57] investigated mono and hybrid nanofluids

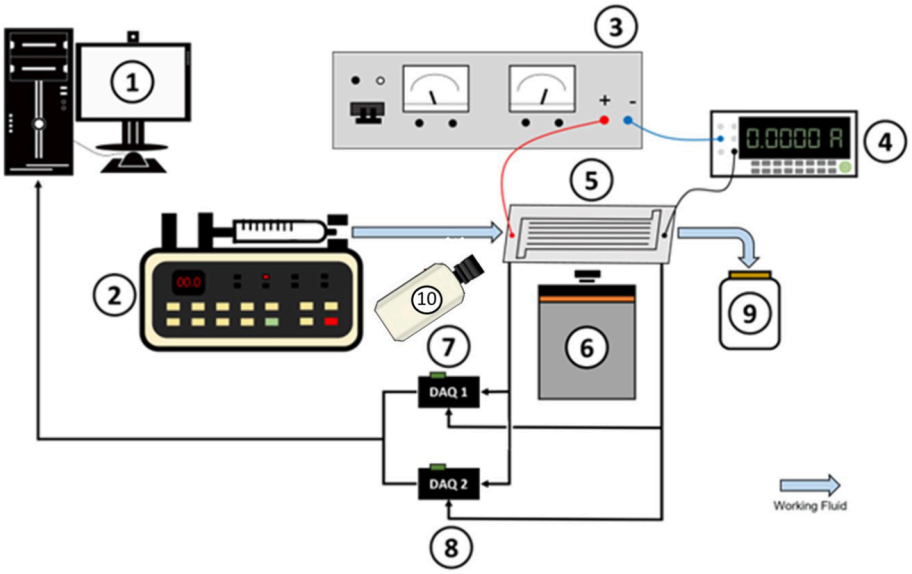

Fig. 1. Schematic of the experimental setup: (1) Computer; (2) Syringe pump; (3) DC power supply; (4) Multimeter; (5) Microchannel system; (6) Thermographic camera; (7) DAQ 1; (8) DAQ 2; (9) Fluid reservoir; (10) High-speed camera.

containing B_4C and TiB_2 nanoparticles at 2 wt% nanoadditive concentration, using PG/W 20/80 wt% as base fluid, to analyze the convection process in a double pipe heat exchanger.

The current challenge, especially for hybrid nanofluids, is to understand in detail the complex mechanisms that present nanoparticles composed of two or more materials. Guan et al. [58], analyzed the relationship between the thermal conductivity and the nanolayer density and the diffusion coefficient.

However, the detailed comprehension of the relationship between the type of nanoparticles, surfactant concentration, microchannel geometries and their complicated dependency on hydraulic and heat transfer properties remains a significant motivation for further investigation in nanofluid applications [59–62].

Alkasmoul et al. [63] studied the behaviour of the heat transfer and hydraulic features for various nanofluids on their cooling performances in MCHs. Recently, Maghrabie et al. [64] investigated the benefits of using nanofluids for cooling electronic components. They analyzed the heat transfer mechanism to avoid the hot spots on the electronic systems. Vinoth et al. [65] examined the heat transfer enhancement in oblique finned curved microchannel comparing different nanofluids: DI water, Al_2O_3/water nanofluid and Al_2O_3 + CuO/water.

Martinez et al. [66] demonstrated the importance of the use of nanofluids and of the reduction of the microchannel height on thermal performance, at low Reynolds numbers in MCHs. For a nanoparticles concentration of 3 wt% and a Reynolds number of 200, they obtained convective heat transfer coefficients higher than 19.66%, when compared to the base fluid.

An interesting recent work [67] analyzed the performance of Al_2O_3-water nanofluids in a heat sink and demonstrated that Al_2O_3/water nanofluids have a higher heat transfer coefficient by 51%, 61 %, and 68 % (respectively for volumetric concentrations of 0.25%, 0.5%, and 0.75%) with respect to distilled water.

Ho et al. [68] tested as working fluids the ultrapure water and water-based alumina nanofluids for volume concentrations of alumina nanoparticles from 0.5 and 1.0% in a microchannel heat sink.

Their results underlined the direct link between the nanoparticles raising and the thermal conductivity of the fluid and the heat transfer rate.

Concerning the working fluid, recently the investigation of the hydrofluoroether (HFE) thermophysical behaviour in microchannel systems is also addressed as this is considered an experimental fluid of great interest from many scientists. Yang et al. [69] investigated the flow boiling heat transfer of HFE-7000 in nanowire-coated microchannels. Alam et al. [70] analyzed the flow boiling HFE-7100 in silicon nanowire and plain wall microchannels. They observed that a higher mass flux of HFE-7100 reduces the impact of SiNW on system performances and Critical Heat Flux (CHF). Dang et al. [71] studied the flow boiling heat transfer and pressure drop of HFE-7000 in continuous and segmented microchannels. Cui and Liu [72] improved the flow boiling of HFE-7100 in picosecond laser fabricated copper MCHs. Bortolin et al. [73] analyzed the flow boiling of R134a and HFE-7000 in a single silicon microchannel with microstructured sidewalls. A new wicked-microchannel is proposed from Li [74] to improve the heat transfer performance of HFE-7100.

Cen et al. [75] proved that the process of boiling HFE-7100 on copper foams under overflow conditions significantly improved the cooling capacity during the transition from liquid to vapor phase.

Lee et al. [76] studied the influence of system pressure on flow boiling in microchannels. Ates et al. [77] studied a dielectric fluid HFE-7000. They obtained average boiling heat transfer coefficients over effective heat fluxes ranging from 50 to 1300 kW/m2 and mass fluxes from 125 to 280 kg/m^2.

Recently Mlakar et al. [78] underlined the influence of the surface variations on nucleate boiling performance.

Soleimani et al. [79] evaluated the thermal performance of the cooling process by two-phase flow boiling of Al_2O_3 HFE-7100 nanofluids in a microchannel heat sink. They evaluated the heat transfer efficiency in the case of the single-phase flow and two-phase boiling flow compared for the same operating conditions. They also observed that the addition of nanoparticles to the HFE-7100 improves the local heat transfer of flow boiling. To evaluate the benefits of a two-phase flow, the working fluid often considered is HFE-7100, whose zero-ozone depletion potential and boiling point (61 °C, at ambient pressure) make it a suitable option for this kind of work. In contrast with water, for example, HFE-7100 is a dielectric fluid, so in case of leaks or any malfunction, there is no harm caused to the electronic components of the system. In this context, the current research aims to investigate flow boiling of pure liquids and nanofluids on microchannel-based heat sinks. First, specific two phase-flow patterns and their main issues related to cooling applications are discussed, followed by a discussion on nanofluids as a potential player to enhance heat transfer. Different experimental tests are developed to examine the geometrical effects using water, HFE7100

Table 1
Different geometries selected from those made by Martins [81].

Structure	Wc (mm)	W_w (mm)	W (mm)	L (mm)	H_c (mm)	n of channels	D_h $\frac{2W_cH_c}{W_c+H_c}$(mm)	Total Area of passage (mm^2)	Total Area of cooling (mm^2)
1	0.25	0.25	10.25	20	1	21	0.4	5.25	205
2	0.25	0.50	10.00	20	1	14	0.4	3.50	200
3	0.25	0.75	10.25	20	1	11	0.4	2.75	205
4	0.50	0.25	10.25	20	1	14	0.7	7.00	205
5	0.50	0.50	10.50	20	1	11	0.7	5.50	210
6	0.50	0.75	10.50	20	1	9	0.7	4.50	210
7	0.75	0.25	10.75	20	1	11	0.9	8.25	215
8	0.75	0.50	10.75	20	1	9	0.9	6.75	215
9	0.75	0.75	9.75	20	1	7	0.9	5.25	195

and water based nanofluids, with nanoparticles of silver, gold and alumina.

The novelty of this research compared to previous studies lies in the use of a MEMS device capable of improving heat transfer by taking into the account both the use of nanofluid as working fluid and the microchannel heat sink geometry, with or without phase change. Furthermore, there is an unusual use and concentration of gold and silver nanofluids which are explored here.

2. Experimental methods

2.1. Experimental apparatus

The experimental setup comprises several components. An AISI304 stainless-steel sheet (65 mm × 21 mm) is placed beneath the microchannels heat sink. The sheet is 20 μm thick and is fitted with two copper plates at its end. These plates are connected to a wire that carries current from an HP 6274B DC power supply, generating an imposed heat flux by Joule effect. Additionally, the microchannel based heat sink is held in place by two acrylic plates. Fig. 1 shows a schematic of the different parts and devices used in the experimental arrangement, as well as how they are interconnected. The syringe pump Harvard Apparatus 22 (2) is used to pump the working fluid into the microchannel system (5), where it is heated by an AISI304 stainless-steel sheet and subsequently stored in the reservoir (9). The imposed heat flux is created by a current generated using the power supply (3), which is adjusted to the desired values based on the measurements from a Tektronix DMM4020 digital multimeter (4). The temperature distribution of the steel sheet is monitored using an Onca MWIR-InSb-320 thermographic camera (6), which is placed under the microchannel system, pointing upwards, and manually focused. The fluid's inlet and outlet temperatures are recorded using two type K thermocouples coupled with a DT9828 data acquisition device (DAQ) (7), while the pressure difference between the inlet and outlet sections is measured by an Omega PX26-005DV pressure sensor and sent to another DT9828 DAQ (8). The QuickDAQ Base Package software is used to record the pressure difference and fluid temperature values. The data captured by the thermographic camera and the DAQ devices are sent to the laptop (1), for further analysis using Matlab routines developed in-house. Moreover, a high-speed camera (Phantom v4.2 High Speed Camera) (10), equipped with a Leica microscope lens with 4x magnification, is used to observe and record the flow boiling inside the microchannels based heat sink, working at 1000fps. A calibration factor of 45 μm/pixel was obtained for the current optical configuration. It is important to note that a single channel configuration was used to study the flow boiling patterns, while multichannel configurations are used further to evaluate the global performance of the heat sink. The microchannels based heat sinks were made from Polydimethylsiloxane (PDMS) to allow optical access.

Details on the experimental setup are described in Moita et al. [80].

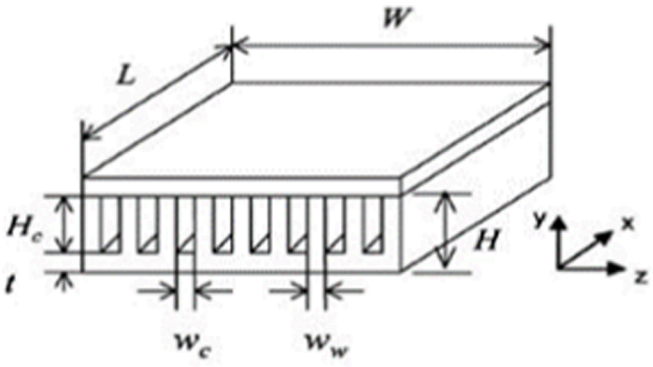

Fig. 2. Schematic of the microchannel heat sink (adapted from Halelfadl et al. [82]).

2.1.1. Microchannel based heat sinks

A key element for these experiments is represented by the microchannel based heat sinks. The two-phase flow studies were conducted using a single microchannel with fixed dimensions of 20 mm in length (L) and 1 mm in height (H_c). The width of the channels (w_c) and the thickness of the walls (w_w) were varied, as indicated in Table 1.

Additional tests were conducted to assess the influence of microchannel geometry on the cooling process by varying the dimensions of the channels. These different microchannel geometries were previously fabricated using additive manufacturing, with various molds made from PLA (polylactic acid) and produced using an Ultimaker 3D printer.

The total area of passage can be calculated by multiplying the number of channels by the channel's width and channel's height. On the other hand, the total area cooling is calculated by multiplying the width by the length of a single channel. During this work, it was decided to maintain the wall width while changing the width of each channel. Therefore, the geometries used are summarized in Table 1, following those defined by Martins [81]. The main dimensions of the channels and the heat sink are identified in Fig. 2. *L, W, H,* and *t* represent the length, width, height and the substrate thickness of the microchannel heat sink, respectively. w_c, w_w and H_c denote the channel width, wall width and channel height, respectively. The hydraulic diameter, D_h, is also provided in Table 1.

Table 2
Properties of HFE7100 at atmospheric pressure and 61 °C [83].

Property	Value
Liquid density ρ [kg/m^3]	1418.602
Liquid dynamic viscosity μ [Pa.s]	4.3E-4
Specific heat C_p [KJ/(kgK)]	1183
Thermal conductivity k [W/(mK)]	0.069
Latent heat h_{fg} [kJ/kg]	111.6
Surface tension σ [mN/m]	13.6

Table 3
Characteristics and thermal properties of the different nanoparticles used.

Material	*Shape*	*Size [nm]*	*ρp [kg/ m3]*	*Kp [W/(m. K)]*	*Cp,p [kJ/(kg. K)]*
Al_2O_3	Spherical	40–50	3970	46	0.765
Ag	Triangular	68–74	10,500	429	0.235
Au	Spherical	40–50	19,300	317	0.129

Table 4
Thermal properties of the different nanofluids used at 20 °C and 1 atm.

Fluid	ρ_{eff} [kg/ m^3]	μ_{eff} [mPa.s]	k_{eff} [W/ (m.K)]	cp_{eff} [kJ/ (kg.K)]	$\beta_{eff} \times 10^4$ [°C$_{-1}$]
Water	998.230	0.980	0.620	4.184	2.100
Al_2O_3 1 wt%	1005.759	0.986	0.625	4.150	2.095
Ag 1 wt%	1007.346	0.982	0.622	4.145	2.098
Au 1 wt%	1007.787	0.981	0.621	4.143	2.099
Au 0.75 wt%	1005.380	0.981	0.621	4.154	2.099
Au 0.5 wt %	1002.986	0.981	0.620	4.164	2.099

2.2. Experimental procedure and working conditions

The heat flux is controlled by imposing a DC current to the stainless-steel sheet. The same procedure is used to heat both the single channel and the multichannel heat sinks. To observe the flow boiling patterns the imposed heat flux could be as high as 4.2 kW/m^2. The volumetric flow rate was varied between 1 mL/min and 5 mL/min. In this case, the working fluid is the HFE7100, from 3 M, whose properties are summarized in Table 2.

The experiments performed to examine the geometrical effects involved the use of water, HFE7100, water based nanofluids with nanoparticles of silver, gold and alumina. In that case, the heat flux was different than those imposed when identifying the flow regimes and was fixed to 3.59 kW/m^2. The volumetric flow rate was varied between 10 mL/min and 40 mL/min. Alumina nanofluids were prepared according to the two-step method described in Santos [84], while gold and silver nanofluids were prepared using the single-step method also described in Santos [84]. All the nanofluids were firstly tested with an initial concentration fixed at 1%wt. Afterwards, to investigate the influence of the nanoparticle concentration in the heat flux, three different concentrations of the gold nanofluid were used (0.5 wt%, 0.75 wt% and the initial 1 wt%).

Table 3 shows the thermal properties of the nanoparticles used, while Table 4 shows the thermal properties of the different fluids that were used throughout our experiments in this part of the work. For the nanofluids, the effective density (ρ_{eff}), viscosity (μ_{eff}), thermal conductivity (k_{eff}) and specific heat (cp_{eff}) were calculated using equations (1–4) proposed by Khanafer and Vafai [85], Einstein [86], Maxwell [87] and Xuan and Roetzel [88], respectively:

$$\rho_{eff} = (1-\varnothing_p)\rho_f + \varnothing_p\rho_p \quad (1)$$

$$\mu_{eff} = (1+2.5\varnothing_p)\mu_f \quad (2)$$

$$k_{eff} = k_f + \frac{3\varnothing_p(k_p-k_f)}{k_p+2k_f-\varnothing_p(k_p-k_f)} \quad (3)$$

$$Cp_f = \frac{Cp_f\rho_f(1-\varnothing_p)+Cp_f\rho_f\varnothing_p}{\rho_{eff}} \quad (4)$$

The thermal expansion β_{eff} is the tendency of a material to increase its volume as the temperature changes, and can be expressed by by equation 5 [85]:

Table 5
Mean surface tension and standard deviation (SD) of all working fluids used in this work, at room temperature.

Fluid	σ [mN/m]	(SD)
Water	74.580	0.771
Al_2O_3 1 wt%	71.928	1.949
Ag 1 wt%	74.178	0.897
Au 1 wt%	73.428	0.637
Au 0.75 wt%	73.188	1.239
Au 0.5 wt%	73.409	0.623

$$\beta eff = \beta f(1-\varnothing_p)+\beta_p\varnothing_p \quad (5)$$

As seen in Table 4, the properties of the working fluids are very similar. Surface tension is a particularly important property, which can be easily affected by surfactants and nanoparticles, so it was measured for the nanofluids. Surface tension was measured using the pendant drop method in an optical tensiometer THETA, from Attention, at room temperature (20–24 °C). A droplet was generated at the tip of a needle using a fixed liquid volume of approximately 1–2 μL. Afterwards, a video of 10 s at 12 fps was recorded. Using the captured images, the software was able to calculate the surface tension of the fluid used by force balance. The values given in Table 5 are averaged from fifteen measures, to minimize errors in the measurements.

When examining the values for the surface tension of the fluids, it is impossible to establish relations between the different working fluids or nanoparticle concentrations. There are also some errors associated with each measurement, as indicated by the different values for the standard deviation. However, the associated errors are generally small. The similarity between the various surface tension values can also be explained by the fact that the different working fluids share the same base fluid (distilled water) in their composition. Therefore, it can be concluded that the introduction of, at least, small percentages of nanoparticles in the base fluid does not cause significant changes in its surface tension. These values are also in accordance with the results reported by Santos [84] and Maly et al. [89].

2.3. Experimental procedure

For the experiments with the single channel, to identify the boiling regimes, the flow rate was first fixed with a progressive increase of the imposed heat flux, and vice-versa. Each observed regime had to be reproducible in similar conditions at least 3 times.

For the experiments with the multichannel heat sink, the procedure was divided into two different routines. The first routine corresponded to experiments at ambient temperature, with no heat flux applied to the steel-sheet. This routine aimed to analyze and validate the assembly of the system.

The objective of the second routine was to study the cooling performance of the heat sink, particularly with the nanofluids. Therefore, in this routine, the tests were conducted at ambient temperature with a constant heat flux imposed on the steel sheet.

The first routine was repeated for water and the Al_2O_3 nanofluid and can be described by the following steps:

1. The syringe was filled with the working fluid at ambient temperature;
2. The desired flow rate was set on the syringe pump and turned on;
3. When the temperature of the steel sheet reached a constant value, i.e, steady state condition, the software controlling the acquisition boards was initiated. Data were collected, including the inlet and outlet temperatures, as well as the pressure difference between these two points, at 10 Hz during 60 s, resulting in 600 different values for each data type;
4. When the acquisition routine finished, the syringe pump was turned off;

5. The acquired data was saved as a.csv file;

6. Excess fluid was removed from the system piping, and the routine was repeated.

The second routine was carried out for the Al_2O_3, Au and Ag nanofluids. This process can be described in the steps bellow:

1. The syringe was filled with the working fluid at ambient temperature;

2. The desired flow rate was set on the syringe pump;

3. The DC power supply was turned on, providing a fixed current of 6.5A, corresponding to 3592.69 W/m^2;

4. The routine for data acquisition was initiated to record the temperature evolution of the steel-sheet at a rate of 4–6 fps;

5. Once the steel sheet reached a temperature of around 65 °C, the syringe pump was turned on to initiate the cooling process;

6. When the flow reached steady-state i.e. the temperature of the steel-sheet was observed to reach a constant value on the software, another acquisition routine was initiated, collecting data from the thermocouples and pressure sensor at 10 Hz for 60 s;

2.4. Data treatment

In terms of internal flow, pressure drop inside the microchannels was evaluated based on the pressure drop, which was further treated to obtain the Fanning friction factor, f given by:

$$f = \frac{2\tau}{\rho u_m^2} = \frac{D_h \Delta_p}{2L\rho u_m^2} \tag{5}$$

With τ being the shear stress on the tube walls, D_h the hydraulic diameter, Δp the pressure losses, u_m the mean flow velocity and ρ the density of the fluid. The higher the channel's pressure drop, the higher the costs associated with the respective system. This is due to the increase in pumping power (P_p) of the system, evaluated through equation:

$$P_{p=n} \dot{Q}_i \Delta_p \tag{6}$$

Where $\dot{Q}_i$ is the volumetric flow rate in each channel and n is the total number of channels in the system.

As for the heat transfer calculations, when considering an imposed heat flux to the surface, the heat transfer mechanisms can be studied. This allows for a better understanding of the fluid flow inside our heat exchanger. To achieve the surface heat flux on a thin heated surface (q''), Kenning and Yan [90] define the heat flux as:

$$q'' = q_0'' + k_h \delta_h \left(\frac{\partial^2 T}{\partial x^2} + \frac{\partial^2 T}{\partial y^2} \right) - \rho_{h C p_h \delta_h} \frac{\partial T}{\partial t} \tag{7}$$

Where q_0'' is the imposed heat flux from the heater. The constants k_h, ρ_h, Cp_h and δ_h are the conductivity, density, specific heat and thickness of the heated surface.

Then the heat removed by the liquid is obtained from an energy balance, being the heat transfer coefficient simply obtained by:

$$h = \frac{q''}{T_s - \frac{T_{in}+T_{out}}{2}} \tag{8}$$

Being T_s the surface temperature and T_{in}, T_{out} the liquid temperature at the entrance and exit of the heat sink. The temperature values taken from the analysis of the thermal images are treated as detailed in Mendes [91].

All the quantities obtained were averaged from 5 tests performed under similar working conditions.

As for the analysis of the flow patterns, each regime was identified from at least 3 experiments performed under similar working conditions, for a single channel. Bubble diameters were evaluated at three sections of the channel (beginning, middle and end of the channel) considering fifteen imagens in each section, for at least 3 experiments performed under similar working conditions.

Table 6
Equipment uncertainties for experimental tests.

Equipment	Uncertainty
Onca MWIR-InSb-320 Camera	± 0.5 °C
Harvard Apparatus 22 Syringe Pump	± 0.035%
Omega PX26-005DV Pressure Sensor	± 0.34 kPa
Type K Thermocouple	± 0.5 °C
DT9828 DAQ	± 20 μV
HP 6274B DC Power Supply	± 0.05°
Tektronix DMM4020 Digital Multimeter	± 0.00001A

Table 7
Accounted Heat Losses.

q″[W/m^2]	1026	1696	2403
Tsurf [°C]	59	71	84
Heat Losses [W/m^2]	133.2	175.3	220.8

2.5. Uncertainty analysis

The uncertainties of the frequency count and of the detachment diameters and velocities measures are ± 1 pixel. This means that the uncertainty associated with the bubble detachment diameter is ± 45 μm and the uncertainty for bubble detachment velocity is ± 0.0029 m/s. The main uncertainties of the other parameters are shown in Table 6.

Throughout the experimental work, there are errors associated with the equipment used. To assess the solidness of the experimental results, there is a need to quantify these errors. Uncertainties related to the equipment used in the experimental work can be seen in Table 6.

The heat losses are shown in Table 7, where surface temperatures were measured, and an equivalent resistance model was considered. This model includes a 6 mm acrylic plate underneath the sheet with a conductivity of 0.17 W/(m.K) and natural convection to air at 21 °C.

3. Results and discussion

The results presented and discussed here are divided into two main groups. The first group focuses on two-phase flow working conditions in the microchannel based heat sink. Firstly, the flow-boiling regimes are identified and discussed for the working conditions covered in this study. Then, the heat transfer mechanisms are analyzed in terms of the benefits of heat transfer enhancement (in comparison with single-phase flows) versus the problems resulting from flow instabilities. Overall, the main conclusion for the working conditions explored here is that they do not recommend the use of two-phase flow conditions in the heat sink. Following this, additional strategies are addressed in a final section, namely the use of nanofluids.

3.1. Two-phase flow regimes and heat transfer in microchannels based heat sinks

In this first section, the boiling patterns are discussed for the working conditions studied here. To ensure the accurate identification of the regimes, the patterns were analyzed in the beginning, middle and end of a single channel. For this phase of the study, three heat fluxes were selected: 1,026 kW/m^2, 1,696 W/m^2, and 2,403 kW/m^2. Additionally, the volumetric flow rates varied between 0.5 mL/min and 1.5 mL/min. Fig. 3 identifies the flow regimes observed. From these, 3 dominant regimes are identified: dispersed bubbles, bubbly and transition to slug flow. The first regime is characterized by small, dispersed bubbles. In the second regime, both small and large bubbles are observed, with coalescence of larger bubbles being more frequently observed. Finally, in the slug flow regime, large masses of vapour cover the section of the channel and start growing in a cylindrical shape. These masses are formed by the coalescence of multiple bubbles and absorb all the vapor

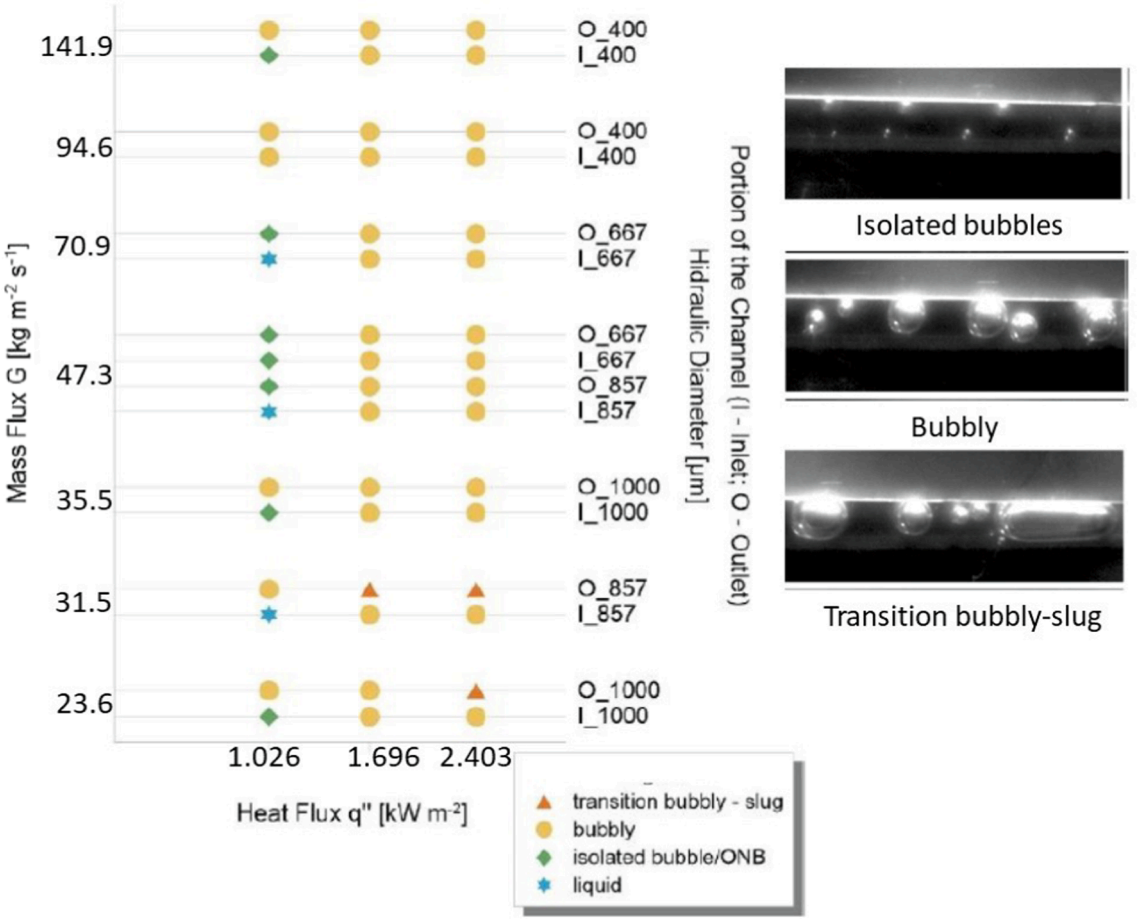

Fig. 3. Flow boiling regimes identified in the working conditions explored in the present study.

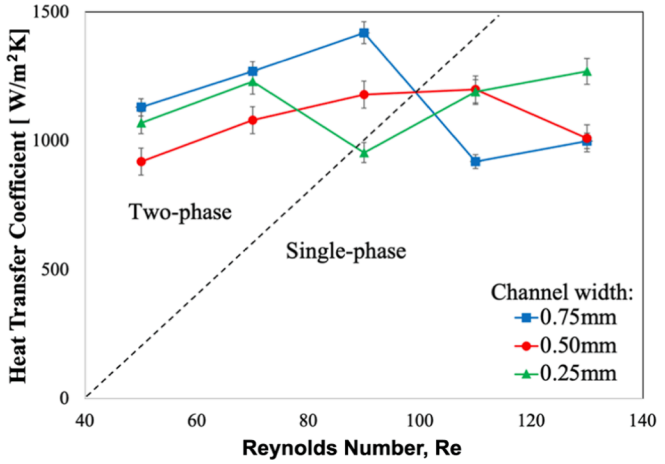

Fig. 4. Heat Transfer coefficient for microchannel based heat sinks, varying the width of the channel.

masses as they pass through activated nucleation sites. Regarding the effect of governing parameters, it is evident that a higher flow rate will lead to a higher frequency of bubbles. It is also observed that a higher heat flux, in general, increases the number of bubbles per second. However, it can also activate so many nucleation regions that the pressure increases, and the flow may be obstructed. This means that for higher heat fluxes, there may be larger bubbles at lower frequencies, due to the occurrence of coalescence. Gravity also plays an important role, as nucleation occurs near the base of the microchannel, causing all bubbles to rise to the top of the channel due to the density difference. Some bubbles can either keep growing or be absorbed by the liquid, as phase change occurs near the liquid–vapour interface.

As bubbles grow with the imposed heat flux and decrease their frequency, clogging is more likely to occur. In fact, since coalescence is more likely to occur under these conditions, slugs may quickly form, raising the pressure and leading to instability and the occurrence of backflow. Therefore, using a large number of thin channels may not be beneficial since, despite the potential for a more uniform wetted area, the occurrence of clogging and instabilities outweighs this potential benefit. This observation seems to be supported by the heat transfer coefficient obtained for a heat sinks with several microchannels. Indeed, Fig. 4 depicts the heat transfer coefficient as a function of the Reynolds number for microchannel heat sinks with fixed wall width (in this case, equal to 0.75 mm) and square side lengths of the channel area of 250 μm, 500 μm and 750 μm. Overall, the best results are obtained for the heat sink with the largest channel side.

Furthermore, it is not evident that two-phase flow conditions consistently lead to higher heat transfer coefficients, given the large fluctuation in the results. While there is an obvious increase in the heat transfer coefficients as phase change occurs, it is mainly observed in geometries with larger channels. On the other hand, the smaller width channels do not show significant improvement in heat transfer with two-phase flow and exhibit larger fluctuations associated with clogging caused by vapor and the occurrence of backflow. There is an observable increase in pressure drops, but fluctuations are also present due to bubble generation in the channels. Considering this analysis, alternative strategies should be explored.

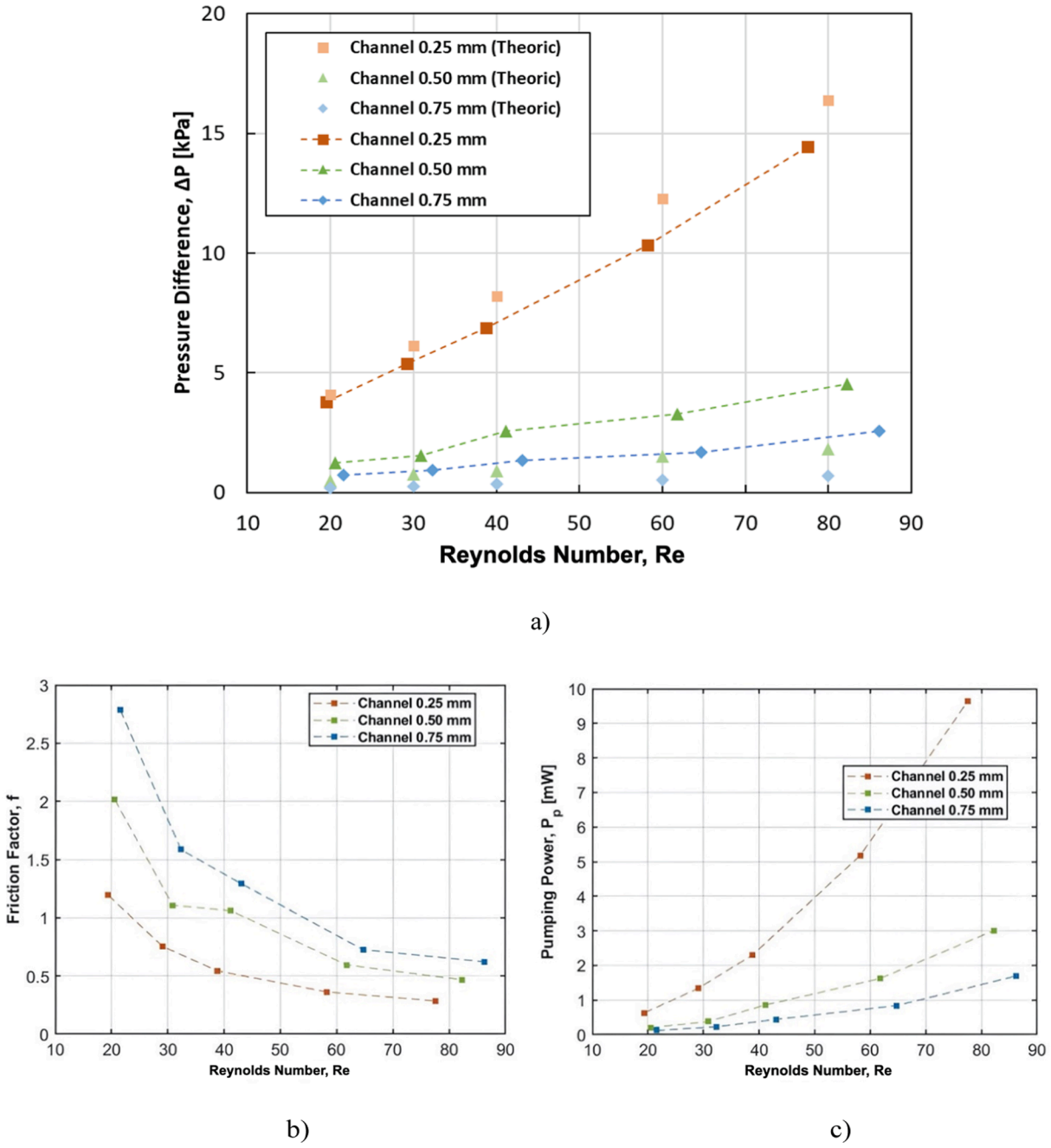

Fig. 5. A) pressure drop, b) fanning friction factor and c) required pumping power for the water flow in pdms microchannel based heat sinks with varying channel width.

3.2. Alternative cooling strategies: The use of nanofluids

Following the analysis performed so far, it is difficult to recommend the use of working conditions leading to two-phase flows, given that the benefits in terms of heat transfer coefficients and heat fluxes obtained, when compared to single-phase flows are not enough to compensate the problems caused by the flow instabilities.

Hence, additional strategies are discussed to close the analysis and recommend the working conditions for the microchannel based heat sink being developed. Firstly, the experimental setup is validated comparing the pressure drop, Fanning friction factor and pumping power for the microchannel based heat sink working with water at ambient temperature, to the results previously reported by Martins [81] and Carvalho [92]. Three different geometries, from Table 1, were tested: geometry 2, with a channel width of 0.25 mm and an aspect ratio AR of 4; geometry 5, with a channel width of 0.50 mm and an AR of 2, and finally, geometry 8, with a channel width of 0.75 mm and an AR of 1.33. In all these cases, the wall width was fixed at 0.50 mm, the length of the channels was 20 mm and the height of the channels was 1 mm. Therefore, the main parameter varying here is the channel width, ranging between 0.25 mm and 0.75 mm. According to the literature [46,48], the aspect ratio directly influences the pressure drop in microchannels. Higher aspect ratios would result in higher pressure drops and, consequently, higher friction factors and pumping power. However, the use of nanofluids (discussed at the end of this section) should not have a significant influence on the pressure drop when compared to water [93,94].

Fig. 5 (a)-(c) depict, respectively, the pressure drop, friction factor and pumping power obtained for water flowing in the aforementioned geometries as a function of the Reynolds number, Re.

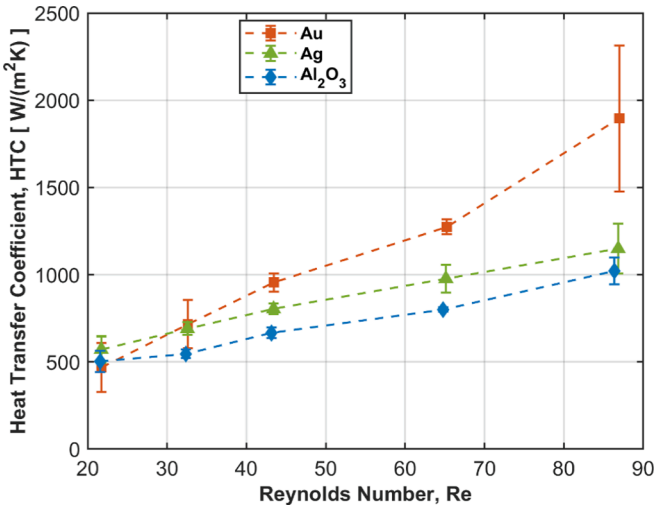

Fig. 6. Heat transfer coefficient as a function of the Reynolds number for water-Al_2O_3, water-Ag and water-Au nanofluids (1% wt%), using the heat sink with geometry 8.

When looking at Fig. 5(a), it is clear to see that, for all microchannel heat sinks tested, the pressure drop increases with the increasing volumetric flow rate (which increases the Reynolds number). However, the friction factor shows an inverse behaviour, decreasing with the growth in the flow rate, meaning that the inertial forces of the flow are larger than the local shear stress (see Fig. 5b). As shown in Fig. 5(c), the trend of the pumping power is analogous to that of the pressure drop, increasing exponentially with the flow rate and implying rising pumping energy costs. These trends are in agreement with those reported in [71,82]. Furthermore, experimental results were compared against theoretical values deducted by the Darcy–Weisbach equation given by:

$$\frac{\Delta p}{L} = \frac{128}{\pi}\frac{\mu Q}{D_c^4} \tag{9}$$

The results are close enough to the theoretical values to validate the experiments.

3.2.1. *Effect of nanoparticles' material and concentration*

In this subsection, the stainless-steel sheet was heated up to 65–70 °C, and the tests were performed in geometry 8. It is worth noting that the selection of the geometry used for the nanofluid tests was not random. Previous work addressed and extensive study of the effect of the channels' geometry (e.g. [90,91]), which demonstrated a better equilibrium between the increase in the heat transfer coefficient and the pressure drops for larger channels. Hence, geometry 8 was chosen based on this previous extensive analysis.

Thermal images were taken with the thermographic camera and the processed data was used to compute the experimental Nusselt number, *Nu*, which was compared to the empirical correlations proposed by Peng and Peterson [95] and by Xuan and Li [96]:

$$Nu = 0.1165\left(\frac{D_h}{Wc}\right)^{0.81} AR^{-0.79} Re^{0.62} Pr^{1/3} \tag{10}$$

$$Nu_{nf} = 0.4328\left(1 + 11.285 \varnothing_{np}^{0.754} Pe_{np}^{0.218}\right) Re_{nf}^{0.333} Pr_{nf}^{0.4} \tag{11}$$

Where $D_h = 4Area/Perimeter$ is the hydraulic diameter, AR is the aspect ratio, nf stands for nanofluid and np for nanoparticle. Pr is the Prandtl number and Pe is the Peclet number.

The Peng and Peterson [95] correlation analyzed the single-phase forced convective heat transfer and flow characteristics of water in microchannel structures/plates with small rectangular channels and distinct geometric configurations, while the Xuan and Li [96] correlation considered the microconvection and microdiffusion effects of the

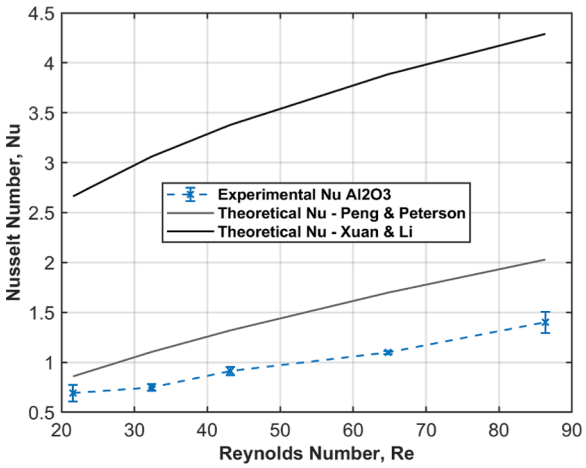

a)

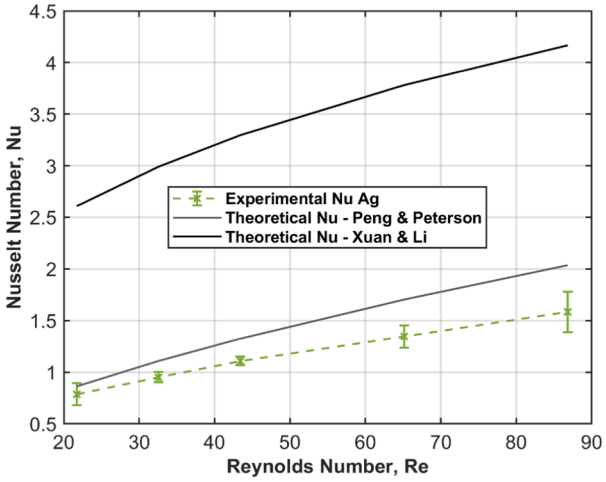

b)

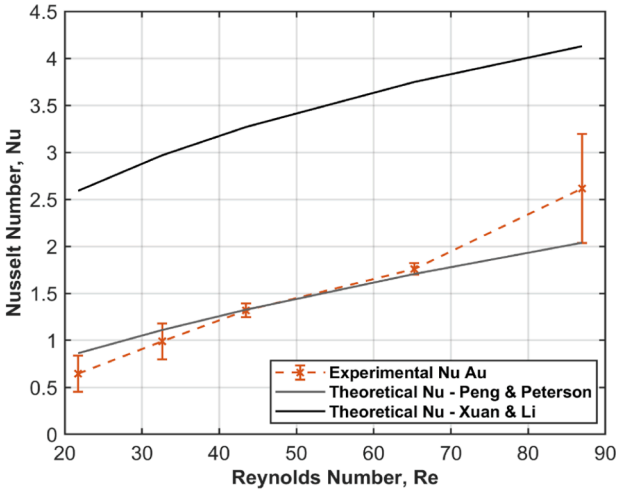

c)

Fig 7. Nusselt number, as a function of the Reynolds number for: a) water-Al_2O_3, b)water-Ag and c) water-Au nanofluids, (1% wt), using the heat sink with geometry 8.

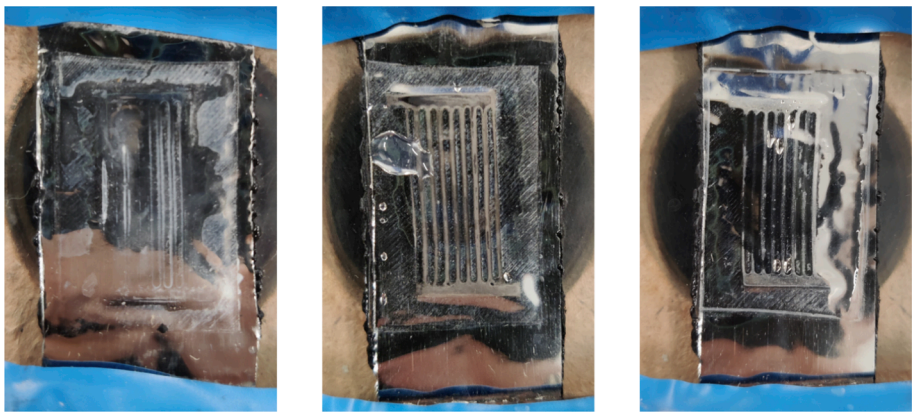

a) b) c)

Fig. 8. Sedimentation on the stainless-steel sheet for: a) water-Al_2O_3, b) water-Ag and c) water-Au nanofluids, after a day of experiments.

suspended nanoparticles in the nanofluids during the single-phase flow. Both correlations were developed from experimental investigations.

Figs. 6 and 7 depict the thermal behaviour of the three nanofluid used (water-Al_2O_3 1%wt, water-Ag 1%wt and water-Au 1%wt) as a function of the Reynolds number. The Nusselt number, Nu, is compared with the empirical correlations proposed in [85–86].

As expected, the three nanofluids exhibit a similar thermal behaviour, directly proportional to the increasing Reynolds number, Re. According to Fig. 6, the nanofluid that demonstrated the best heat transfer coefficient overall was the one composed of gold nanoparticles, having only the worst thermal behaviour for the lowest volumetric flow rate compared to the water-Ag and water-Al_2O_3 nanofluids.

The increase in heat transfer from nanofluids is generally associated with an increase in their thermal conductivity, as can be seen in [97], but in the present study, the nanofluids used has practically identical thermal properties, see Table 4. However, another characteristic that can influence the heat transfer coefficient is the size of the nanoparticle, although there is still no consensus among the scientific community about it [98]. As shown in the work [98], it is believed that the reduction of the size of the nanoparticles increases the effective surface area, thickens the interfacial layer and increases Brownian motion, which would increase the thermal conductivity of the nanofluid. So, the Au nanofluid composed of smaller nanoparticles would have better heat transfer compared to the Ag nanofluid, even though Ag has a higher k than Au. The distinct behavior observed for the gold nanofluid at the lowest volumetric flow rate may be associated with the fact that gold nanoparticles are more prone to agglomeration and sedimentation compared to silver nanoparticles (gold is denser). Agglomeration decreases the efficiency of heat transfer. In addition, the agglomerated particles have difficulty interacting with the base fluid, which impairs thermal dissipation. However, this negative effect tends to disappear as the system flow rate increases.

Similarly, as anticipated, the Nusselt number, Nu, also increases with the Reynolds number, Re, and is larger for the water-Au nanofluid, followed by the silver and alumina nanofluids, respectively, as shown in Fig. 7. The thermal properties of the three nanofluids are very similar, as indicated in Table 4, due to the low particle concentrations used. Because of this, the Nusselt numbers estimated from the empirical correlations also agree well for the three fluids, particularly with the nanofluid using the gold particles. Also, the correlation from Xuan and Li [86] shows a better agreement with the experimental values, in comparison with that proposed by Peng and Peterson [95] which is over 100% overestimating the results.

The fact of considering the effects of the suspension of nanoparticles during the flow of nanofluids it is possible one of the reasons why the Xuan and Li [86] correlation presented more satisfactory results when compared to the Peng and Peterson [95].

Both the alumina (Fig. 7a) and silver (Fig. 7b) based nanofluids, for all flow rates, depict lower experimental values for the Nusselt number in contrast with the empirical correlations. Inversely, the gold nanofluid (Fig. 7c) starts with lower Nu values but then overcomes the estimations from [95].

Another important aspect to consider when evaluating the nanofluids is their tendency for sedimentation or fluid stability. To study this, a photo of the stainless-steel sheet was taken after a day of experiments for each nanofluid, as depicted Fig. 8. It is possible to see that the three nanofluids sedimented. Nevertheless, the water-Au nanofluid (Fig. 8c) appears to be the most stable nanofluid, while, on the other hand, the water-Al_2O_3 shows the greatest amount of nanoparticle buildup on the stainless-steel sheet.

This can be further asserted by looking at Fig. 9, which shows the large amount of sedimentation on the syringe used to pump the fluid into the microchannel heat exchanger, when using alumina nanoparticles. Comparably, the gold and silver nanofluids barely showed nanoparticles buildup in the syringe.

With both the thermal behaviour and stability of the nanofluid

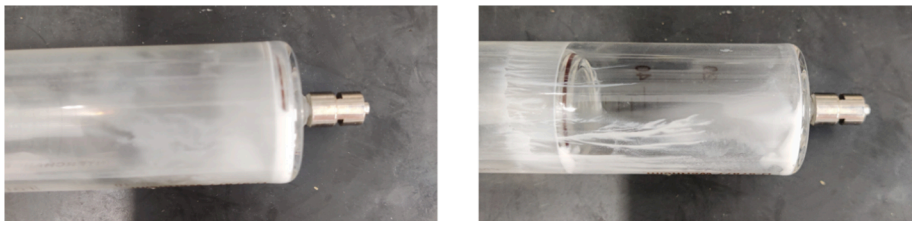

Fig. 9. Sedimentation on the syringe for water-Al_2O_3 nanofluid after a day of experiments.

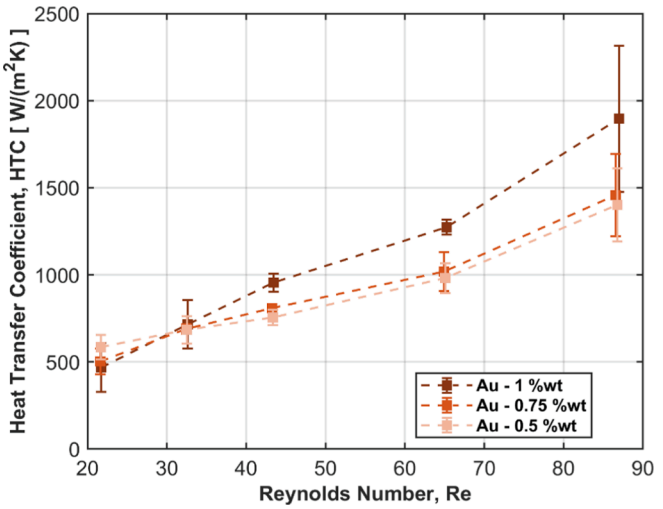

Fig. 10. Heat transfer coefficient as a function of Reynolds number, for water-Au nanofluids at different nanoparticles concentration, using geometry 8.

evaluated, the water-gold nanofluid was selected to conduct the last part of the experimental work, which consisted in inferring on the effect of varying the nanoparticles' concentration in the fluid.

3.2.2. *Effect of nanoparticles' concentration*

Given that the best results were obtained with the water-Au, nanofluid, different nanoparticles' concentrations were tested using this nanofluid, namely 0.5%wt, 0.75%wt and 1%wt. Fig. 10 depicts the effect of nanoparticles' concentration in the heat transfer coefficient. The costs and effort associated to an optimization task are out of the scope of the current work, so the optimum gold concentration could not be assessed. Detailed investigations will be presented in future work. Comparison between gold and silver was not performed either, due to the same argument. However, previous work, (e.g. [84]) addressed a systematic study on the effect of nanoparticles concentration from both Ag and Au. Overall, the results showed a similar behaviour of Au and Ag nanofluids with the increase in nanoparticles concentration, overall depicting better heat transfer coefficients for gold.

In Fig. 11, it is possible to notice that the thermal behaviour of the nanofluid is, on average, better for the largest particle concentration, only having the worst results for the slowest volumetric flow rate. Additionally, the heat transfer coefficient of the two smallest particle concentrations increases with similar slopes throughout the graph. However, for the highest nanoparticle concentration, the increase in the heat transfer coefficient is significantly greater than that of the other concentrations, being over 50% higher for the fastest flow rate.

Regarding the Nusselt number, and in agreement with the previous analysis, our experimental results closely match the correlation proposed by Xuan and Li [86], following it almost perfectly. The experimental data follows trends reported in the literature, with the largest nanoparticle concentration having the better thermal behaviour. Therefore, even for very small concentrations ($\phi \ll 1\%$), the effect of nanoparticles on cooling performance is tremendous, as seen in this section, and becomes more pronounced at higher flow rates. As aforementioned, one of the largest problems associated with nanofluids is sedimentation. For this reason, in order to increase their reliability in cooling and heat transfer mechanisms, it is extremely important to study these fluids with the purpose of increasing their stability, without diminishing their thermal properties, and to find the optimal concentration for the largest cooling performance, with little to no sedimentation.

Similar conclusions were also reported by Bowers et al. [96], although used nanoparticles different from those presented here. Bowers et al. [96], conducted experimental studies on flow and heat transfer of

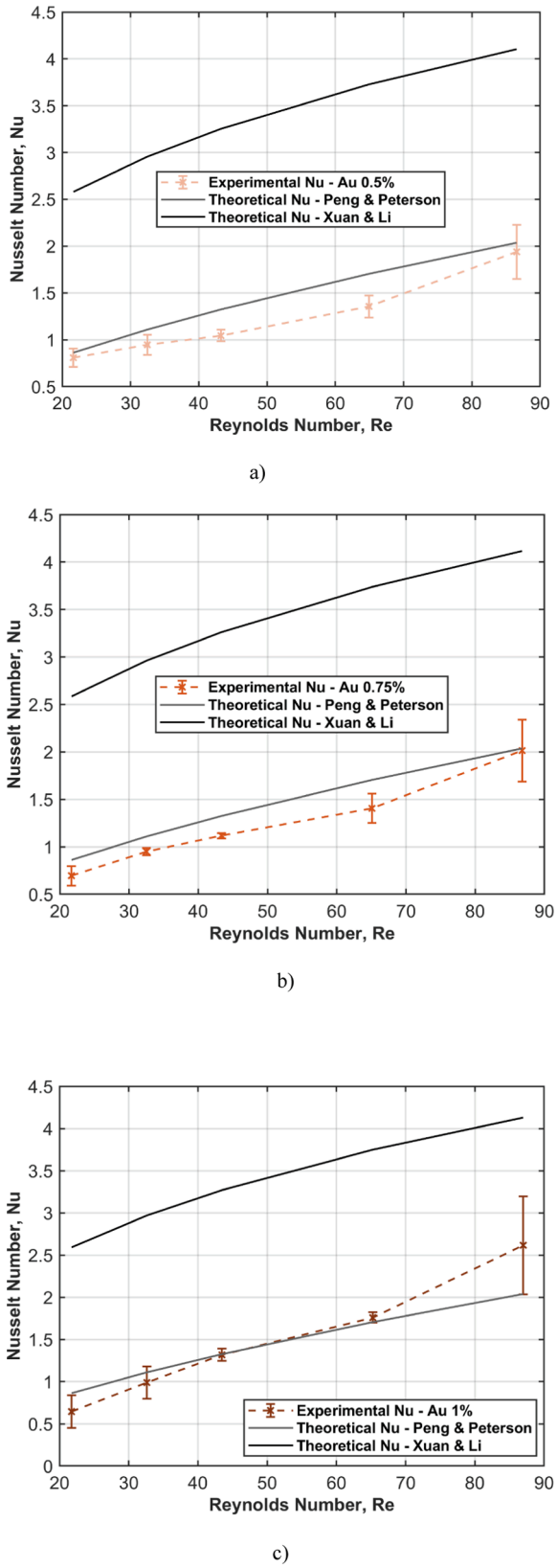

Fig. 11. Nusselt number for a nanoparticle concentration of 0.5%wt (a), 0.75% wt (b) and 1%wt (c), using water-Au nanofluid as the working fluid and utilizing geometry 8.

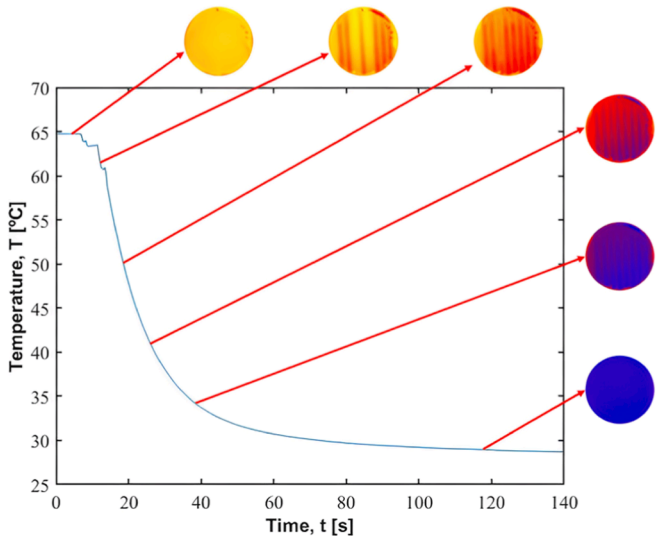

Fig. 12. Cooling of the steel sheet overtime, with images from the IR camera (Onca MWIR-InSb-320) for different timestamps, for a flow rate of 15 mL/min and for geometry 8 (channel width of 0.75 mm), using water-Al_2O_3 as the working fluid.

silica and alumina nanofluids in microchannels. They demonstrated an increase in heat transfer with increasing Reynolds number and microchannel hydraulic diameter. However, it was observed that most experiments showed a larger increase in pumping power requirements compared to heat transfer enhancements.

3.3. Thermographic analysis

In this section, the various thermal images captured by the thermographic camera, Onca MWIR-InSb-320, are analyzed and displayed for a better understanding of the heat transfer processes that occurred in the stainless-steel sheet when using the various nanofluids as the cooling liquid. Therefore, the main objective of this section is to examine the temperature drop of the steel sheet and corresponding cooling time associated with it.

Fig. 12 shows the temperature evolution of the steel sheet with thermographic images captured at specific instants during the cooling phase. This image is relative to the experiment that used Water-Alumina nanofluid as the working fluid, for a microchannel structure with 0.75 mm of channel width (geometry 8) and with a flow rate of 15 mL/min.

It is possible to observe, in Fig. 12, that the stainless-steel sheet takes more than a full minute to stabilize its temperature, reaching this point at around 90 s for this particular case. Additionally, the initial drop in temperature (from 65 to around 63 °C) is related to the presence of air

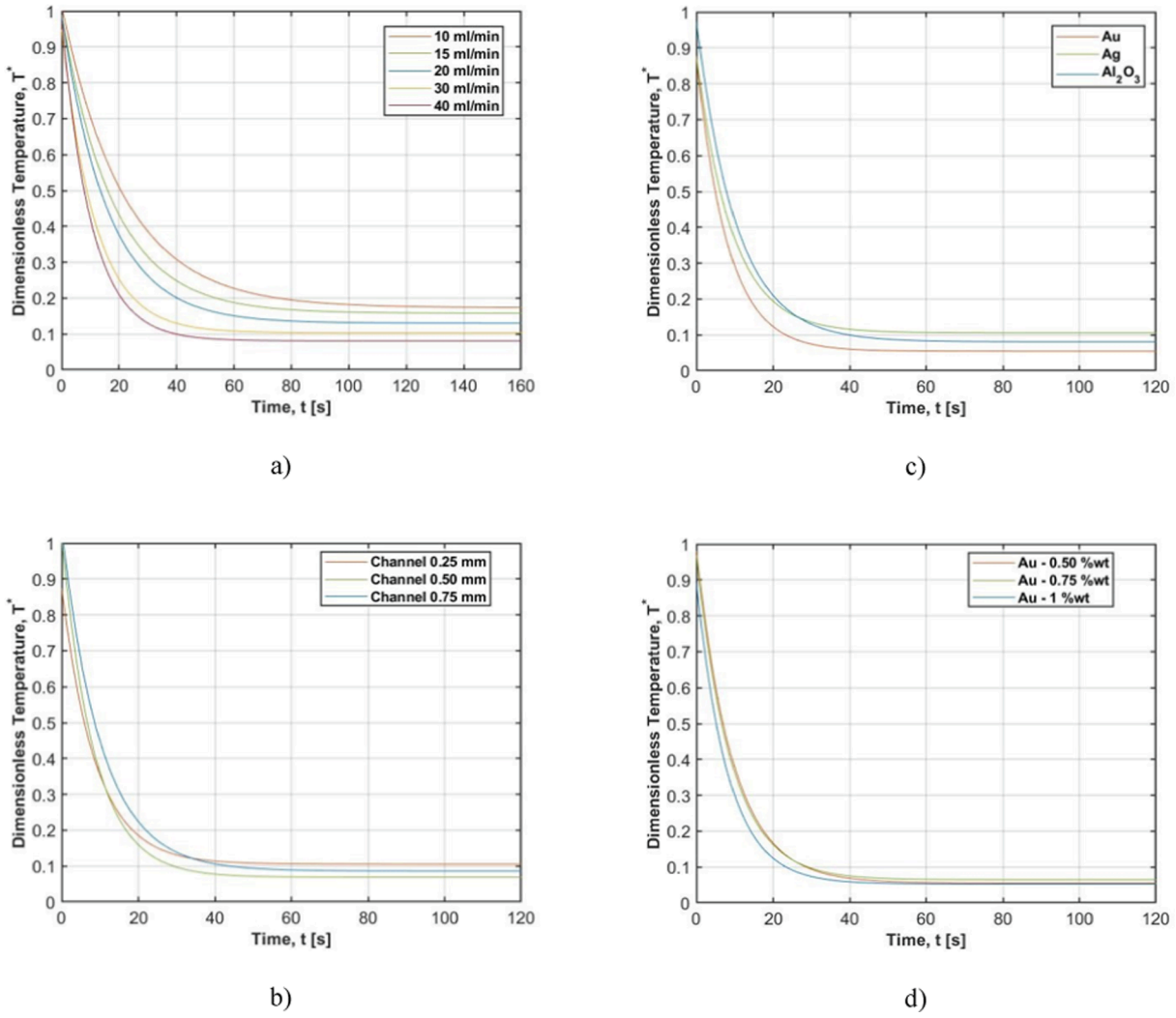

Fig. 13. Cooling of the stainless-steel sheet overtime, using a dimensionless temperature (T*), for: a) different flow rates, b) different heat sink geometries, c) different nanofluids and d) different nanoparticles' concentration.

inside the pipes circulating through the microchannels, with the fluid entering the structure at the 15 s mark. The red lines that emerge in the second circular image correspond to the cooler areas, i.e, the microchannels where the nanofluid is circulating. As the steel sheet cools down, the images show darker shades of red, gradually transitioning to blue. Once the stainless-steel sheet temperature completely stabilizes last circular image, the channel lines in the image captured by the thermographic camera become almost imperceptible. In the next step, to better perceive and better understand the temperature evolution, various different cases are compared to each other. For this purpose, data from the steel sheet is transformed into a dimensionless temperature data from the steel sheet is transformed into a dimensionless temperature variable (T^*), given by:

$$T^* = \frac{T - T_{amb}}{T_{max} - T_{amb}} \tag{11}$$

With T_{max} being the maximum temperature achieved by the stainless-steel sheet during the heating process, which is 70 °C, and T_{amb} being the average ambient temperature, with a value of 22 °C. In addition, with the aim of assisting in the data comparison and analysis and to describe the average cooling behaviour of each case, since they are repeated five times, corresponding exponential tendency lines were traced, as seen in Fig. 13.

For comparing the different cooling times for different flow rates, the data used was relative to geometry 8 (in Table 2) while using the Al_2O_3 nanofluid. For the remaining three graphs, the experimental results correspond to the highest volumetric flow rate (40 mL/min) used during the experimental work. Upon analyzing the different temperature evolution data, it is evident that, for the most part, the cases that showed a better heat transfer coefficient, as discussed in the previous paragraphs, also exhibit lower stabilization temperatures and a faster cooling time. This is particularly noticeable in the graph comparing the various nanoparticle concentrations (Fig. 13d), where the temperatures at which the steel sheet stabilizes and corresponding cooling times are very similar. Moreover, this graph further confirms our analysis from the previous paragraphs, demonstrating that even for the lowest particle concentration used, the Water-Gold nanofluid outperforms the remaining fluids tested during the experimental work.

4. Conclusions

The present study evaluated the benefits and challenges of two-phase flows, specifically flow boiling of pure liquids and nanofluids, on microchannel heat sinks for cooling applications. The study analyzed different two-phase flow patterns, identified associated issues during the volumetric flow rates, and explored the potential of nanoparticles to enhance heat transfer. Were used Alumina (Al_2O_3), gold (Au), and silver (Ag) nanoparticles in concentrations of 0.5%wt, 0.75%wt and 1%wt. The key findings that can be drawn from this study are:

- Low concentrations of nanoparticles ($\phi \ll 1\%$) significantly enhanced heat transfer mechanisms and offered a cost-effective and efficient alternative for microchannel heat sink cooling applications;
- Two-phase flow conditions in microchannel heat sinks did not provide significant benefits for cooling applications;
- The analysis of flow boiling regimes and heat transfer mechanisms revealed occurrence of flow instabilities, clogging, and backflow outweighed the potential advantages of two-phase flow;
- The choice of nanoparticle kind and concentration had a notable impact on the thermal behavior of nanofluids;
- Gold nanofluids demonstrated better cooling performance compared to alumina and silver nanofluids;
- The thermal behavior of nanofluids, as observed through thermographic analysis, indicated that the use of water-gold nanofluids led to faster cooling and lower stabilization temperatures compared to other nanofluids tested;
- The use of dimensionless temperature analysis, at thermal analyzed, allowed for effective comparison and characterization of cooling behavior across different flow rates, heat sink geometries, nanofluids, and nanoparticle concentrations.

Declaration of Competing Interest

The authors declare that they have no known competing financial interests or personal relationships that could have appeared to influence the work reported in this paper.

Data availability

Data will be made available on request.

Acknowledgements

Authors acknowledge to Fundação para a Ciência e Tecnologia (FCT) for partially financing the research through project PTDC/EMETED/7801/2020 and to Portuguese Army – Ministério da Defesa, for financing project CINAMIL COOLUAV – Cooling system for electronics and batteries for military unmanned vehicles. Mr. Pedro Pontes also acknowledges FCT for supporting his PhD fellowship (Ref. SFRH/BD/149286/2019).

References

[1] J.X. Wang, W.G. Kai, X. Sheng, S.N., Wang,, Review of aerospace-oriented spray cooling technology, Progress in Airspace Sci 116 (2020), 100635.
[2] Army Technology: Drones in Aerospace and Defence: Macroeconomic Trends (army-technology.com).
[3] Z. Qia, Y. Zhenga, J. Wei, X. Yu, X. Jia, J. Liu, L. Chen, J. Miao, C. Li, Surface treatment of an applied novel all-diamond microchannel heat sink for heat transfer performance enhancement, Appl. Therm. Eng. 177 (2020), 115489, https://doi.org/10.1016/j.applthermaleng.2020.115489.
[4] Y. Alihosseini, M.Z. Targhi, M.M. Heyhat, N. Ghorbani, Effect of a micro heat sink geometric design on thermo-hydraulic performance: A review, Appl. Therm. Eng. 170 (2020), 114974.
[5] K. Sienski, R. Eden, D. Schaefer, 3-D electronic interconnect packaging, IEEE Aerospace Appl. Conference 10 (1996) 363–373.
[6] B.H. Salman, H.A. Mohammed, K.M. Munisamy, A.S. Kherbeet, Characteristics of heat transfer and fluid flow in microtube and microchannel using conventional fluids and nanofluids: A review, Rene. Sust. Energ. Rev. 28 (2013) 848–880.
[7] A. Sakanova, S. Yin, J. Zhao, J.M. Wu, K.C. Leong, Optimization and comparison of double-layer and double-side micro-channel heat sinks with nanofluid for power electronics cooling, Appl. Therm. Eng. 65 (2014) 124–134, https://doi.org/10.1016/j.applthermaleng.2014.01.005.
[8] S. Wu, K. Zhang, G. Song, J. Zhu, B. Yao, F. Li, Study on the performance of a miniscale channel heat sink with Y-shaped unit channels based on entransy analysis, Appl. Therm. Eng. 209 (2022), 118295, https://doi.org/10.1016/j.applthermaleng.2022.118295.
[9] J. Wu, J. Zhao, J. Lei, B. Liu, Effectiveness of nanofluid on improving the performance of microchannel heat sink, Appl. Therm. Eng. 101 (2016) 402–412, https://doi.org/10.1016/j.applthermaleng.2016.01.1141359-4311.
[10] S.P. Jang, S.U.S. Choi, Cooling performance of a microchannel heat sink with nanofluids, Appl. Therm. Eng. 26 (2006) 2457–2463, https://doi.org/10.1016/j.applthermaleng.2006.02.036.
[11] S.Y. Qin, R.Y. Ji, C.M. Yang, L.W. Jin, C. Yang, Y. Wang, X.Z. Meng, Experimental study on the thermal characteristics of a 3D thermosyphon heat sink, Appl. Therm. Eng. (2023), https://doi.org/10.1016/j.applthermaleng.2023.120193.
[12] X. Zhuang, Y. Xie, X. Li, S. Yue, H. Wang, H. Wang, P. Yu, Experimental investigation on flow boiling of HFE-7100 in a microchannel with pin fin array, Appl. Therm. Eng. (2023), https://doi.org/10.1016/j.applthermaleng.2023.120180.
[13] M. Dooley, N. Lui, R. Newman, C. Lui, Aircraft Thermal Management -Heat Sink Challenge, SAE Technical Paper (2014–01-2193, 2014,), https://doi.org/10.4271/2014-01-2193.
[14] P. Smakulski, S. Pietrowicz, A review of the capabilities of high heat flux removal by porous materials, microchannels and spray cooling techniques, Applied Thermal Eng. 34 (2016) 636–646, https://doi.org/10.1016/j.applthermaleng.2016.05.096.
[15] G. Marseglia, M Sanches, APC Ribeiro, ALN Moreira, AS Moita. Thermofluid characterization of nanofluids in spray cooling. Applied Thermal Engineering, 210, 118411. 2022.https://doi.org/10.1016/j.applthermaleng.2022.118411.
[16] X. Zhang, R. Tiwari, A.H. Shooshtari, M.M. Ohadi, An additively manufactured metallic manifold-microchannel heat exchanger for high temperature applications, Appl. Therm. Eng. 143 (2018) 899–908, https://doi.org/10.1016/j.applthermaleng.2018.08.032.

[17] D.B. Tuckerman, R.F.W. Pease, High-performance heat sinking for VLSI[J], IEEE Electron Device Lett. 2 (5) (1981) 126–129, https://doi.org/10.1109/EDL.1981.25367.
[18] W.S. Ling, W. Zhou, C.Z. Liu, F. Zhou, D. Yuan, J.L. Huang, Structure and geometric dimension optimization of interlaced microchannel for heat transfer performance enhancement, Appl. Therm. Eng. 170 (2020), 115011, https://doi.org/10.1016/j.applthermaleng.2020.115011.
[19] M.W. Wambsganss, J.A. Jendrzejczyk, e D. M. France,, «wo-Phase flow patterns and transitions in a small, horizontal, rectangular channel, Int. J. Multiph. Flow 17 (3) (1991) 327–342.
[20] J. Lee e I. Mudawar,, Low-temperature two-phase microchannel cooling for high-heat-flux thermal management of defense electronics», IEEE Trans. Components Packag. Technol. 32 (2) (2009) 453–465.
[21] W. Li, J. Ma, T. Alam, F. Yang, J. Khan, e C. Li,, Flow boiling of HFE-7100 in silicon microchannels integrated with multiple micro-nozzles and reentry micro-cavities», Int. J. Heat Mass Transf. 123 (2018) 354–366.
[22] J. Ma, W. Li, C. Ren, J.A. Khan, e C. Li,, Realizing highly coordinated, rapid and sustainable nucleate boiling in microchannels on HFE-7100, Int. J. Heat Mass Transf. 133 (2019) 1219–1229.
[23] T. Harirchian e S. V. Garimella,, Effects of channel dimension, heat flux, and mass flux on flow boiling regimes in microchannels, Int. J. Multiph. Flow 35 (4) (2009) 349–362.
[24] S.G. Kandlikar, Heat transfer mechanisms during flow boiling in microchannels, J. Heat Transfer 126 (1) (2004) 8–16.
[25] S. G. Kandlikar, S. Garimella, D. Li, S. Colin, e M. King, Heat Transfer and Fluid Flow in Minichannels and Microchannels. 2014.
[26] G. Bovesecchi, S. Corasaniti, G. Costanza, F. Piccotti, M. Potenza, M.E. Tata, Heat Conduction and Microconvection in Nanofluids: Comparison between Theoretical Models and Experimental Results, Aerospace 9 (2022) 608, https://doi.org/10.3390/aerospace9100608.
[27] H.B. Kulkarni, M.M. Nadakatti, S.C. Kulkarni, R.M. Kulkarni, Investigations on effect of nanofluid based minimum quantity lubrication technique for surface milling of Al7075-T6 aerospace alloy, Mater. Today:. Proc. 27 (2020) 251–256, https://doi.org/10.1016/j.matpr.2019.10.127.
[28] W. Jamshed, A. K. Alanazi, S. S. P. M. Isa c, R. Banerjee, M. R. Eid, K. S. Nisar, H. Alshahrei, M. Goodarzi, Thermal efficiency enhancement of solar aircraft by utilizing unsteady hybrid nanofluid: A single-phase optimized entropy analysis, Sustainable Energy Technologies and Assessments 52 (2022), 101898, https://doi.org/10.1016/j.seta.2021.101898.
[29] A. Sakanova, K.J. Tseng, Comparison of pin-fin and finned shape heat sink for power electronics in future aircraft, Appl. Therm. Eng. 136 (2018) 364–374, https://doi.org/10.1016/j.applthermaleng.2018.03.020.
[30] F.R. Siddiqui, C.Y. Tso, H. Qiu, C.Y.H. Chao, S.C. Fu, Hybrid nanofluid spray cooling performance and its residue surface effects: Toward thermal management of high heat flux devices, Appl. Therm. Eng. 211 (2022), 118454, https://doi.org/10.1016/j.applthermaleng.2022.11845.
[31] S. Liua, S. Ma, Y. Liu, Y. Wang, Analysis of the energy conversion properties and applications of Nanofluids: A review, Energy Rep. 8 (2022) 175–184, https://doi.org/10.1016/j.egyr.2022.10.207.
[32] W. Yu, H. Xie, A review on nanofluids: Preparation, stability mechanisms, and applications, J. Nanomater. 2012 (Jan. 2012), https://doi.org/10.1155/2012/435873.
[33] B. Bhanvase, D. Barai, Introduction to nanofluids, in: Nanofluids for Heat and Mass Transfer:Fundamentals, Sustainable Manufacturing and Applications, Chapter 1, Academic Press, 2021, pp. 3–42. ISBN: 978-0-12-821955-3.
[34] T.J. Choi, S.H. Kim, S.P. Jang, D.J. Yang, Y.M. Byeon, Heat transfer enhancement of a radiator with mass-producing nanofluids (EG/water-based Al2O3 nanofluids) for cooling a 100 kW high power system, Appl. Therm. Eng. 180 (2020), 115780, https://doi.org/10.1016/j.applthermaleng.2020.115780.
[35] F. Fan, C. Qi, J. Tang, Q. Liu, X. Wang, Y. Yan, A novel thermal efficiency analysis on the thermo-hydraulic performance of nanofluids in an improved heat exchange system under adjustable magnetic field, Appl. Therm. Eng. 179 (2020), 115688, https://doi.org/10.1016/j.applthermaleng.2020.115688.
[36] T.C. Paul, R. Mahamud, J.A. Khan, Multiphase modeling approach for ionic liquids (ILs) based nanofluids: Improving the performance of heat transfer fluids (HTFs), Appl. Therm. Eng. 149 (2019) 165–172, https://doi.org/10.1016/j.applthermaleng.2018.12.039.
[37] M. Bahiraei, R. Rahmani, A. Yaghoobi, E. Khodabandeh, R. Mashayekhi, M. Amanid, Recent research contributions concerning use of nanofluids in heat exchangers: A critical review, Appl. Therm. Eng. 133 (2018) 137–159, https://doi.org/10.1016/j.applthermaleng.2018.01.041.
[38] S. Aberoumand, A. Jafarimoghaddam, M. Moravej, H. Aberoumand, K. Javaherde, Experimental study on the rheological behavior of silver-heat transfer oil nanofluid and suggesting two empirical based correlations for thermal conductivity and viscosity of oil based nanofluids, Appl. Therm. Eng. 101 (2016) 362–372, https://doi.org/10.1016/j.applthermaleng.2016.01.148.
[39] B. Li, Y. Lin, L. Zhu, W. Zhang, Effects of non-Newtonian behaviour on the thermal performance of nanofluids in a horizontal channel with discrete regions of heating and cooling, Appl. Therm. Eng. 94 (2016) 404–412, https://doi.org/10.1016/j.applthermaleng.2015.10.148.
[40] B. Ruan, X. Gao, H. Meng, Numerical modeling of turbulent heat transfer of a nanofluids at supercritical pressure, Applied Thermal Engineering 113 (2017) 994–1003, develophttps://doi.org/10.1016/j.applthermaleng.2016.11.092.
[41] E. Hosseinirad, F. Hormozi, New correlations to predict the thermal and hydraulic performance of different longitudinal pin fins as vortex generator in miniature channel: Utilizing MWCNT-water and Al2O3-water nanofluids, Appl. Therm. Eng. 118 (2017) 199–213, https://doi.org/10.1016/j.applthermaleng.2017.02.1.
[42] S.K. Pathak, R. Kumar, V. Goel, A.K. Pandey, V.V. Tyagi, Recent advancements in thermal performance of nano-fluids charged heat pipes used for thermal management applications: A comprehensive review, Appl. Therm. Eng. 216 (2022), 119023, https://doi.org/10.1016/j.applthermaleng.2022.119023.
[43] S.U.S. Choi, J.A. Eastman, Enhancing thermal conductivity of fluids with nano-particles, ASME, 1995.
[44] R.L. Hamilton, O.K. Crosser, Thermal Conductivity of Heterogeneous Two-Component Systems, Ind. Eng. Chem. Fundamen. 1 (3) (1962) 187–191, https://doi.org/10.1021/i160003a005.
[45] H. Masuda, A. Ebata, K. Teramae, N. Hishinuma, Alteration of thermal conductivity and viscosity of liquid by dispersing ultra-fine particles (Dispersion of Al2O3, SiO2 and TiO2 ultra-fine particles), NetsuBussei (Japan) 7 (1993) 227–233, https://doi.org/10.2963/jjtp.7.227].
[46] M.S. Khan, M. Abid, H.M. Ali, K.P. Ambera, M.A. Bashir, S. Javed, Comparative performance assessment of solar dish assisted s-CO2 Brayton cycle using nanofluids, Appl. Therm. Eng. 148 (2019) 295–306, https://doi.org/10.1016/j.applthermaleng.2018.11.021.
[47] M. Esmaeili, K. Sadeghy, M. Moghaddami, Heat transfer enhancement of wavy channels using Al2O3 nanoparticles, J. Enhanced Heat Transfer 17 (2) (2010) 139–151.
[48] D. Yang, B. Sun, T. Xu, B. Liu, H. Li, Experimental and numerical study on the flow and heat transfer characteristic of nanofluid in the recirculation zone of backward-facing step microchannels, Appl. Therm. Eng. 199 (2021), 117527, https://doi.org/10.1016/j.applthermaleng.2021.117527.
[49] A.S. Kherbeet, H.A. Mohammed, K.M. Munisamy, B.H. Salman, Combined convection nanofluid flow and heat transfer over icroscale forward-facing step, Int. J. Nanoparticles 7 (1) (2014) 1, https://doi.org/10.1504/IJNP.2014.062008.
[50] V. Ozbolat, B. Sahin, Numerical investigations of heat transfer enhancement of water-based Al2O3 nanofluids in a sinusoidal-wall channel, in: ASME International Mechanical Engineering Congress and Exposition. American Society of Mechanical Engineers, 2013, 56345, V08AT09A051.
[51] W. Ajbar, J.A. Hernández, A. Parrales, L. Torres, Thermal efficiency improvement of parabolic trough solar collector using different kinds of hybrid nanofluids, Case Studies in Thermal Engineering 42 (2023), 102759, https://doi.org/10.1016/j.csite.2023.102759.
[52] K. Zheng, A. Raza, A.M. Abed, H. Khursheed, L.F. Seddek, A.H. Ali, A.U. Haq, New fractional approach for the simulation of (Ag) and (TiO2) mixed hybrid nanofluid flowing through a channel: Fractal fractional derivative, Case Studies, Therm. Eng. 45 (2023), 102948.https://doi.org/10.1016/j.csite.2023.102948.
[53] A. Ghafouri, D. Toghraie, Experimental study on thermal conductivity of SiC-ZnO/ethylene glycol hybrid nanofluid: Proposing an optimized multivariate correlation, Journal of the Taiwan Institute of Chemical Engineers, In Press (2023), https://doi.org/10.1016/j.jtice.2023.104824.
[54] J. Shelton, N.K. Saini, S.M. Hasan, Experimental study of the rheological behavior of TiO2-Al2O3/mineral oil hybrid nanofluids, J. Mol. Liq. 380 (2023), 121688, https://doi.org/10.1016/j.molliq.2023.121688.
[55] M. Sepehrnia, K. Mohammadzadeh, M. H. Rozbahani, M. J. Ghiasi, M. Amani, Experimental study, prediction modeling, sensitivity analysis, and optimization of rheological behavior and dynamic viscosity of 5W30 engine oil based SiO2/MWCNT hybrid nanofluid. Ain Shams Engineering Journal, In Press, https://doi.org/10.1016/j.asej.2023.102257.
[56] A. Vardaru, G. Huminic, A. Huminic, C. Fleaca, F. Dumitrache, I. Morjan, Aqueous hybrid nanofluids containing silver-reduced graphene oxide for improving thermo-physical properties, Diam. Relat. Mater. 132 (2023), 109688, https://doi.org/10.1016/j.diamond.2023.109688.
[57] J. P. Vallejo, L. Ansia, U. Calvino¯, M. A. Marcos, J. Fernandez-Seara, L. Lugo, Convection behaviour of mono and hybrid nanofluids containing B4C and TiB2 nanoparticles, International Journal of Thermal Sciences 189 (2023) 108268, https://doi.org/10.1016/j.ijthermalsci.2023.108268.
[58] H. Guan, Q. Su, R. Wang, L. Huang, C. Shao, Z. Zhu, Why can hybrid nanofluid improve thermal conductivity more? A molecular dynamics simulation, Journal of Molecular Liquids 372 (2023), 121178 https://doi.org/10.1016/j.molliq.2022.121178.
[59] M. Sanches, G. Marseglia, A.P.C. Ribeiro, A.L.N. Moreira, A.S. Moita, Nanofluids characterization for spray cooling applications, Symmetry 13 (5) (2021) 788, https://doi.org/10.3390/sym13050788.
[60] H. Waqas, S. Khan, U. Farooq, et al., Thermal transport analysis of six circular microchannel heat sink using nanofluid, Sci. Rep. 12 (2022) 8035, https://doi.org/10.1038/s41598-022-11121-y.
[61] M. Wang, P.S. Dobson, M.C. Paul, Numerical investigation of nanofluid deposition in a microchannel cooling system, Powder Technol. (2023), https://doi.org/10.1016/j.powtec.2023.118582.
[62] Z. Tan, P. Jinb, Y. Zhang, G. Xi. Flow and thermal performance of a multi-jet twisted square microchannel heat sink using CuO-water nanofluids Applied Thermal Engineering 225 (2023),120133.https://doi.org/10.1016/j.applthermaleng.2023.120133.
[63] F.S. Alkasmoul, M. Asaker, A. Almogbel, A. AlSuwailem, Combined effect of thermal and hydraulic performance of different nanofluids on their cooling efficiency in microchannel heat sink, Case Studies in Thermal Engineering 30 (2022), 101776, https://doi.org/10.1016/j.csite.2022.101776.
[64] H. M. Maghrabie, A.G. Olabib, E. Taha Sayed, T. Wilberforce, K. Elsaid, M. H. Doranehgardf, M. Ali Abdelkareem. Microchannel heat sinks with nanofluids for cooling electronic components: Performance enhancement, challenges, and

limitations. Thermal Science and Engineering Progress 37 (2023) 101608, https://doi.org/10.1016/j.tsep.2022.101608.
[65] R. Vinoth, B. Sachuthananthan, A. Vadivel, S. Balakrishnan, A.G. Sagaya Raj, Heat transfer enhancement in oblique finned curved microchannel using hybrid nanofluid, Int. J. Therm. Sci. 183 (2023). 107848.https://doi.org/10.1016/j.ijthermalsci.2022.107848.
[66] T.V.A. Martínez, D.A. Vasco, C.M. García-Herrera, R. Ortega-Aguilera, Numerical study of TiO2-based nanofluids flow in microchannel heat sinks: Effect of the Reynolds number and the microchannel height, Appl. Therm. Eng. 161 (2019), 114130, https://doi.org/10.1016/j.applthermaleng.2019.114130.
[67] C. Kavitha, P.C. Mukeshkumar, C.M. Arun Kumar. Numerical study on the performance of Al2O3/water nanofluids as a coolant in the fin channel heat sink for an electronic device cooling. Materials Today: Proceedings, In press.https://doi.org/10.1016/j.matpr.2023.02.337.
[68] C.J. Ho, J.-K. Peng, T.-F. Yang, S. Rashidi, W.-M. Yan. On the assessment of the thermal performance of microchannel heat sink with nanofluids. International Journal of Heat and Mass Transfer 201 (2023), 123572.https://doi.org/10.1016/j.ijheatmasstransfer.2022.123572.
[69] F. Yang, W. Li, X. Dai, C. Li, Flow boiling heat transfer of HFE-7000 in nanowire-coated microchannels, Appl. Therm. Eng. 93 (2016) 260–268, https://doi.org/10.1016/j.applthermaleng.2015.09.097.
[70] T. Alam, W. Li, W. Chang, F. Yang, J. Khan, C. Li, A comparative study of flow boiling HFE-7100 in silicon nanowire and plain wall microchannels, Int. J. Heat Mass Transf. 124 (2018) 829–840, https://doi.org/10.1016/j.ijheatmasstransfer.2018.04.010.
[71] C. Dang, L. Jia, Q. Peng, L. Yin, Z. Qi, Comparative study of flow boiling heat transfer and pressure drop of HFE-7000 in continuous and segmented microchannels, Int. J. Heat Mass Transf. 148 (2020), 119038, https://doi.org/10.1016/j.ijheatmasstransfer.2019.119038.
[72] P. Cui, Z. Liu, Enhanced flow boiling of HFE-7100 in picosecond laser fabricated copper microchannel heat sink, Int. J. Heat Mass Transf. 175 (2021), 121387, https://doi.org/10.1016/j.ijheatmasstransfer.2021.121387.
[73] S. Bortolin, A. Francescon, G. Ribatski, D. Del Col, Flow boiling of R134a and HFE-7000 in a single silicon microchannel with microstructured sidewalls, Int. J. Heat Mass Transf. 179 (2021), 121653, https://doi.org/10.1016/j.ijheatmasstransfer.2021.121653.
[74] W. Li, K. Luo, C. Li, Y. Joshi, A remarkable CHF of 345W/cm2 is achieved in a wicked-microchannel using HFE-7100, Int. J. Heat Mass Transf. 187 (2022), 122527, https://doi.org/10.1016/j.ijheatmasstransfer.2022.122527.
[75] M. Cen, S. Deng, C. Hu, J. Luo, S. Tan, C. Wang, Y. Wu, Enhanced boiling heat transfer of HFE-7100 on copper foams under overflow conditions, Appl. Therm. Eng. 224 (2023), 120083, https://doi.org/10.1016/j.applthermaleng.2023.120083.
[76] V.Y.S. Lee, T.G. Karayiannis, Influence of system pressure on flow boiling in microchannels, Int. J. Heat Mass Transf. 215 (2023), 124470, https://doi.org/10.1016/j.ijheatmasstransfer.2023.124470.
[77] A. Ateş, S. Çelik, V. Yağcı, M. Çağlar Malyemez, M. Parlak, A.K. Sadaghiani, A. Koşar, Flow boiling of dielectric fluid HFE – 7000 in a minichannel with pin fin structured surfaces, Appl. Therm. Eng. 223 (2023), 120045, https://doi.org/10.1016/j.applthermaleng.2023.120045.
[78] G. Mlakar, C.-N. Huang, C. Kharangate, Effects of surface modifications on pool boiling heat transfer with HFE-7100, International Journal of Thermofluids 17 (2023), 100286, https://doi.org/10.1016/j.ijft.2023.100286.
[79] A. Soleimani, A. Sattari, P. Hanafizadeh, Thermal analysis of a microchannel heat sink cooled by two-phase flow boiling of Al2O3 HFE-7100 nanofluids, Thermal Science and Engineering Progress 20 (2020), 100693, https://doi.org/10.1016/j.tsep.2020.100693.
[80] A.S. Moita, P. Pontes, L. Martins, M. Coelho, O. Carvalho, F.B. Brito, A.L. N. Moreira, Complex fluid flow in microchannels and heat pipes with enhanced surfaces for advanced heat conversion and recovery systems, Energies 15 (2022) 1478. https://www.mdpi.com/1996-1073/15/4/1478.
[81] L.O. Martins, Sistema de refrigeracao por microcanais com escoamento multifasico para paineis solares de alta concentracao, Instituto Superior Tecnico, University of Lisbon, 2020. Master's thesis,.
[82] S. Halelfadl, A.M. Adham, N. Mohd-Ghazali, T. Maŕ e, P. Estell´ e, and R. Ahmad., Optimization of thermal performances and pressure drop of rectangular microchannel heat sink using aqueous carbon nanotubes based nanofluid, Appl. Therm. Eng. 62 (2) (2014) 492–499, https://doi.org/10.1016/j.applthermaleng.2013.08.005.
[83] M, M Thermal Management Fluids: Cool Under Fire - Dielectric heat transfer fluid solutions for military and aerospace applications, Datasheet, 2009.
[84] E. Freitas, P. Pontes, R. Cautela, V. Bahadur, J. Miranda, A.P.C. Ribeiro, R.R. Souza, J.D. Oliveira, J.B. Copetti, R. Lima, J.E. Pereira, A.L.N. Moreira, A.S. Moita, Pool boiling of nanofluids on biphilic surfaces: an experimental and numerical study, Nanomaterials 125 (11) (2021) 1–23, https://doi.org/10.3390/nano11010125.
[85] K. Khanafer, K. Vafai, A critical synthesis of thermophysical characteristics of nanofluids, Int. J. Heat Mass Transf. 54 (19–20) (2011) 4410–4428, https://doi.org/10.1016/j.ijheatmasstransfer.2011.04.048.
[86] A. Einstein, Eine neue bestimmung der moleku ̈ldimensionen, Ann. Phys. 324 (2) (1906) 289–306, https://doi.org/10.1002/andp.19063240204.
[87] C. Maxwell, A Treatise on Electricity and Magnetism, Clarendon press, Oxford, 1873.
[88] Y. Xuan, W. Roetzel, Conceptions for heat transfer correlation of nanofluids, Int. J. Heat Mass Transf. 43 (19) (Oct. 2000) 3701–3707, https://doi.org/10.1016/S0017-9310(99)00369- 5.
[89] M. Maly, A. Moita, J. Jedelsky, A. Ribeiro, A. Moreira, Effect of nanoparticles concentration on the characteristics of nanofluid sprays for cooling applications, J. Therm. Anal. Calorim. 135 (2019) 3375–3386, https://doi.org/10.1007/s10973-018-7444-z.
[90] D. Kenning, Y. Yan, Pool boiling heat transfer on a thin plate: features revealed by liquid crystal thermography, Int. J. Heat Mass Transf. 39 (15) (Oct. 1996) 3117–3137, https://doi.org/10.1016/0017-9310(96)00006-3.
[91] J.F.P. Mendes, Post-processing image techniques for experimental methods in thermography, University of Lisbon, 2021 [MA Thesis].
[92] D.S. Carvalho, Study of the geometry of microchannels based heat sinks to cool high concentrated photovoltaic cells, Instituto Superior Tecnico, University of Lisbon, 2022. Master's thesis,.
[93] R. Zhang, M. Hodes, N. Lower, and R. Wilcoxon. High heat flux, single-phase microchannel cooling. 2014 Semiconductor Thermal Measurement and Management Symposium (SEMI-THERM), pages 1–7, Mar. 2014. doi:10.1109/SEMI-THERM.2014.6892207.
[94] D. Raghuraman, R.T.K. Raj, P. Nagarajan, B. Rao, Influence of aspect ratio on the thermal performance of rectangular shaped micro channel heat sink using cfd code, Alex. Eng. J. 56 (1) (2017) 43–54, https://doi.org/10.1016/j.aej.2016.08.033.
[95] X. Peng, G. Peterson, Convective heat transfer and flow friction for water flow in microchannel structures, Int. J. Heat Mass Transf. 39 (12) (Aug. 1996) 2599–2608, https://doi.org/10.1016/0017-9310(95)00327-4.
[96] J. Bowers, H. Cao, G. Qiao, Q. Li, G. Zhang, E. Mura, Y. Ding, Flow and heat transfer behaviour of nanofluids in microchannels, Progress in Natural Science: Materials Int. 28 (2) (2018) 225–234, https://doi.org/10.1016/j.pnsc.2018.03.005.
[97] R.R. Souza, I.M. Gonçalves, R.O. Rodrigues, G. Minas, J.M. Miranda, A.L. N. Moreira, R. Lima, G. Coutinho, J.E. Pereira, A.S. Moita, Recent advances on the thermal properties and applications of nanofluids: From nanomedicine to renewable energies, Appl. Therm. Eng. 201 (2022), 117725, https://doi.org/10.1016/j.applthermaleng.2021.117725.
[98] I. Gonçalves, R. Souza, G. Coutinho, J. Miranda, A. Moita, J.E. Pereira, A. Moreira, R. Lima, Thermal conductivity of nanofluids: a review on prediction models, controversies and challenges, Appl. Sci. 11 (2021), https://doi.org/10.3390/app11062525.